Exposure of the Hidden Anti-ferromagnetism in Paramagnetic CdSe:Mn Nanocrystals

Shou-Jyun Zou, Sheng-Tsung Wang, Ming-Fan Wu, Wen-Bin Jian, and Shun-Jen Cheng*

Department of Electrophysics, National Chiao Tung University, Hsinchu 300, Taiwan

ABSTRACT We present theoretical and experimental investigations of the magnetism of paramagnetic semiconductor CdSe:Mn nanocrystals and propose an efficient approach to the exposure and analysis of the underlying anti-ferromagnetic interactions between magnetic ions therein. A key advance made here is the development of an analysis method with the exploitation of group theory technique that allows us to distinguish the anti-ferromagnetic interactions between aggregative Mn^{2+} ions from the overall pronounced paramagnetism of magnetic-ion-doped semiconductor nanocrystals. By using the method, we clearly reveal and identify the signatures of anti-ferromagnetism from the measured temperature-dependent magnetisms and furthermore determine the average number of Mn^{2+} ions and the fraction of aggregative ones in the measured CdSe:Mn nanocrystals.

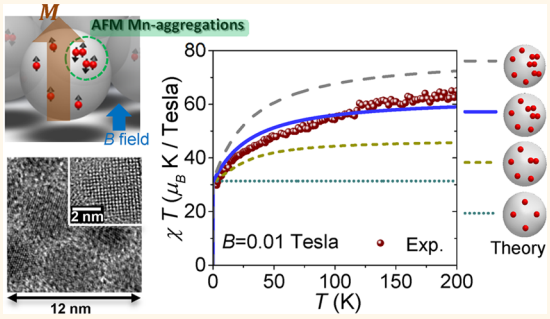

KEYWORDS: anti-ferromagnetism · paramagnetism · magnetic semiconductor nanocrystals · CdSe · Mn

Magnetic-ion-doped semiconductor nanocrystals (NCs) have persistently drawn increasing attention over the years due to their application potential in spintronics and nanomagnetics.[1−4] In general, the magnetism of a semiconductor NC doped with isoelectronic magnetic ion dopants, such as CdSe:Mn NCs, is established mainly by the paramagnetism of magnetic ion dopants themselves, which are possibly subjected to additional anti-ferromagnetic (AFM) interactions if some of them are aggregated.[5−10]

Such an underlying anti-ferromagnetism in a paramagnetic semiconductor is, however, difficult to be fully exposed because it is significant only between nearest neighbor (NN) magnetic ions,[10−12] with a portion of randomly distributed magnetic ion dopants, and likely smeared out by the overall paramagnetism. Nevertheless, the AFM interactions between magnetic ions in magnetic semiconductors have been extensively thought to significantly affect the magnetic features, including the reduced effective Mn concentration,[13,14] fast spin relaxation,[15] and low Curie temperature in the ferromagnetic phase.[16−19]

As a common observed magnetic feature, the number of substitutional magnetic ions in a magnetic semiconductor NC estimated from the measured magnetization is usually lower than the actual supplied amount of magnetic ion dopants. Such a discrepancy could be simply attributed to the loss of magnetic ion dopants in the synthesis processes but also possibly results from the underlying AFM. To reveal the latter origin, one must be able to identify the statistical distribution of the magnetic ions or at least to distinguish the weakly interacting distant magnetic ions and the aggregative ones that are interacting anti-ferromagnetically. Yet, such a delicate consideration for magnetic ion dopants statistically distributed in a NC is actually difficult to achieve both experimentally and theoretically.

Practically, one often mixes the two kinds of magnetic ions (both spatially apart and aggregative magnetic ions) in a magnetic semiconductor and then models the resulting magnetism phenomenologically, in terms of tunable effective magnetic ion concentration, on the basis of mean field theory (MFT).[9,11,13,20] For magnetic-ion-doped semiconductor NCs, the validity of the MFT,

* Address correspondence to sjcheng@mail.nctu.edu.tw.

Received for review October 6, 2014 and accepted December 31, 2014.

Published online December 31, 2014
10.1021/nn5056892

© 2014 American Chemical Society

where all individual magnetic ion spins are smeared out as a single continuous field, still remains an open question. On the other hand, the advanced exact diagonalization (ED) technique, which allows consideration of magnetic ions individually and yields reliable results, is, however, applicable only for a small number of magnetic ions ($N < 10^1$).[21−23] The lack of appropriate theoretical tools for the analysis of magnetic NCs (especially the ones with the moderate number ($N \sim 10^1-10^2$) of Mn ions, as studied in this work) sets an obstacle for more exploration into those intriguing magnetic nanostructures.

In this work, we present theoretical and experimental investigations of the magnetism of CdSe:Mn nanocrystals with the number of Mn^{2+} ions ranging from a few to more than 70. To reveal the underlying AFM in the paramagnetic NCs, we propose an efficient approach to the exposure and analysis of the hidden AFM in the paramagnetism of CdSe:Mn nanocrystals. A key advance made in our theoretical treatment is the development of a solvable model which preserves Mn spins individually and the exploitation of a group theory technique for efficient counting of tremendously high degeneracies of the energy spectrum. With the theoretical aids, we clearly reveal and identify the signatures of AFM from the measured temperature-dependent magnetization of CdSe:Mn NCs with the number of Mn ions as great as ~75. Furthermore, we are able to estimate the average number of substitutional Mn ions and even infer the fraction of the aggregative Mn ions therein. With the employed model extended, the electrical charging effects on the enhancement of the magnetism of CdSe:Mn NCs are also studied and discussed.

RESULTS AND DISCUSSION

In this study, five samples (MCS504, MCS508, MCS515, MCS804, and MCS815) of spherical $Cd_{1-x}Mn_xSe$ NCs of two different sizes (diameters of d = 5 and 8 nm) with various Mn concentrations (x_{dop} = 0.375, 0.75, and 1.5%) were prepared using a high-temperature organic solution approach.[24] Table 1 lists the average diameters (d), estimated Mn concentrations (x_{dop}), and the corresponding average number of Mn ions per NC (N_{dop}) for all the samples. The Mn concentrations, x_{dop}, are estimated according to the supplied dosage of the doping Mn dopants and are controllable during the input for NC synthesis. Behind the specific values of x_{dop}, the Mn ions actually vary in number, NC by NC, and based on the nondestructive magnetization measurements, no further information can account for their spatial distributions. Figure 1a depicts a CdSe:Mn NC in a NC ensemble doped with statistically distributed Mn ions, which as an example consists of four spatially apart Mn ions (referred to as distant Mn ions hereafter) and four spatially close ones (referred to as aggregative Mn ions). One can find the basic descriptions for the method of sample preparation and magnetization measurements in the Methods section. Section S3 of Supporting Information (SI) provides more detailed information about sample synthesis and characterizations.

TABLE 1. Data of the Measured CdSe:Mn Nanocrystal Samples[a]

sample no.	d (nm)	N_{dop}	x_{dop} (%)	N_{eff}	x_{eff} (%)	N_T	x_T (%)
MCS504	5	4.5	0.375	3.0	0.25	3	0.25
MCS508	5	9.0	0.75	5.4	0.45	6	0.50
MCS515	5	18.3	1.5	6.7	0.55	8	0.66
MCS804	8	18.5	0.375	4.2	0.09	8	0.16
MCS815	8	75.0	1.5	45	0.90	75	1.50

[a] Data include the average diameter of the NC (d) and average numbers of doping Mn^{2+} per NC (N_{dop}, N_{eff}, and N_T) estimated by the supplying dopant amount, the measured B-dependent, and the measured T-dependent magnetisms, respectively (see text for details). The corresponding Mn concentrations (x_{dop}, x_{eff}, and x_T) are deduced from the ratio of the estimated numbers of Mn ion and that of total Cd lattice sites (N_{Cd}) of the NC; *i.e.*, $x_{dop/eff/T} \equiv N_{dop/eff/T}/N_{Cd}$.

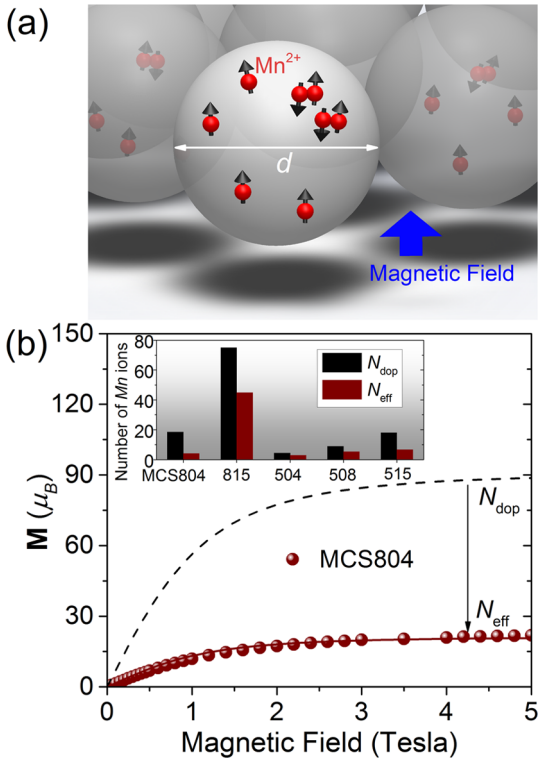

Figure 1. (a) Schematics of the measured CdSe:Mn nanocrystals doped with Mn^{2+} ions that are statistically positioned. (b) Measured magnetizations as functions of the magnetic field of the CdSe:Mn NC ensembles, MCS804. The solid lines (dashed lines) are the magnetizations of ideal paramagnets described by $M = N_{eff} g_{Mn} \mu_B J B_J(g_{Mn}\mu_B B/kT)$ with $N_{eff} = 4.2$ (with $N_{dop} = 18.5$). The inset shows the statistics of the average numbers (N_{dop}) of Mn ions per NC that are estimated from the supplying dopant amounts in the chemical syntheses and the numbers (N_{eff}) of magnetically effective Mn ions per NC that are deduced from the measured magnetizations for the five NC samples. Note that for all samples the N_{eff} values are shown smaller than the N_{dop} values.

Experimental Observations. Figure 1b presents the measured average magnetization per NC of the MCS804

sample as a function of the magnetic field, which is shown to be well-fitted by an ideal paramagnetic magnetization $\mathbf{M} = N_{\text{eff}} g_{\text{Mn}} \mu_B J B_J(g_{\text{Mn}} \mu_B B/kT)$ but with the substitution of another effective number of Mn ions, $N_{\text{eff}} = 4.2$, where $B_J(x)$ is the Brillouin function, $J = 5/2$ is the spin of the Mn ion, $g_{\text{Mn}} = 2.0$ is the g-factor of the Mn ion, B is the external magnetic field, k is the Boltzmann constant, T is the temperature, and μ_B is the Bohr magneton. Note that the corresponding effective Mn concentration, $x_{\text{eff}} \equiv N_{\text{eff}}/N_{\text{Cd}} \approx 0.09\%$, is significantly lower than that of supplied Mn ion dopants, $x_{\text{dop}} \equiv N_{\text{dop}}/N_{\text{Cd}} \approx 0.375\%$, where N_{Cd} is the total number of Cd lattice sites in a CdSe:Mn NC.

To highlight the underestimated Mn concentration, x_{eff}, Figure 1b compares the observed magnetizations fitted with x_{eff} and the one yielded by the Brillouin function formalism with the substitution of x_{dop}. The drastic quantitative difference between the two results indicates significant underestimation of the Mn concentration from the analysis of B-dependent magnetization, a common observed feature of magnetic semiconductor systems.[13,14] Table 1 compares the estimated Mn concentrations (x_{dop} and x_{eff}) by the two means for all the NC samples and confirms the underestimation of x_{eff} and N_{eff} as general phenomena. Graphically, the inset of Figure 1b presents the two estimated average numbers of Mn ions per NC, N_{dop} and N_{eff}, for all measured samples. The possible causes of the reduced x_{eff} and N_{eff} could be the loss of magnetic ion dopants during the synthesis processes or the existence of Mn aggregations, which are AFM-interacting and likely magnetically inactive. In general, both speculated causes are hardly distinguished and confirmed due to a lack of detailed information about the number and distribution of the substitutional magnetic ions in a magnetic NC. Below, we shall present a solvable model and an analysis method for revealing and identifying the signatures of AFM established from aggregated Mn ions from the measured temperature-dependent magnetism of Mn-doped semiconductor NCs.

Model. To conduct a physical analysis for the measured CdSe:Mn NCs with a moderate number of Mn ions (ranging from a few to tens), we encounter the restrictions of the use of the ED and MFT methods that, as previously addressed in the introduction, are applicable only for magnetically doped nanostructures with a small number of magnetic ions or many magnetic ions that are homogeneously distributed, respectively. Here, we attempt to compromise the ED and MFT methods and propose a model Hamiltonian that allows us to deal with, individually, statistically distributed Mn ions and is solvable for magnetic nanostructures with an arbitrary number of Mn ions. The developed model makes use of the fact that Mn−Mn interactions are essentially short-ranged and simplifies the position-dependent Mn−Mn interactions as fixed coupling constants by taking into account only the AFM interactions between *aggregative* Mn ions. Thus, the model Hamiltonian for a magnetic NC with N Mn ions that are composed of P distant and Q aggregative Mn ions ($N = P + Q$) is

$$H_{\text{M}}^{\text{eff}} = -g_{\text{Mn}} \mu_B B \sum_{i=1}^{N} m_i^z + \frac{J_M}{2} \sum_{i(\neq j)=1}^{Q} \sum_{j=1}^{Q} \vec{\text{m}}_i \cdot \vec{\text{m}}_j \quad (1)$$

where $\vec{\text{m}}_i$ (m_i^z) is the spin (z-component of the spin) of the i-th Mn ion and J_M is the constant of effective Mn−Mn coupling between the Q aggregative Mn ions. The first term in eq 1 arises from the couplings between the external magnetic field and *all* N paramagnetic ion dopants, while the second term represents the AFM interactions involving only the Q *aggregative* Mn ions. In the model, we assume that all Mn ions in an aggregation are subjected to the equal effective Mn−Mn interactions to preserve the high permutation symmetry of the spin interactions that is needed later for efficient degeneracy counting using the group theory technique. However, under that assumption, the total strength of the effective anti-ferromagnetic Mn−Mn interactions could be overestimated. To fix the problem, in the use of the model, one needs to appropriately rescale the strength of the effective Mn−Mn interactions according to the specific types of Mn aggregations that exist in the NC. Statistically, as shown in ref 10, the most probable type of Mn ion aggregation could be paired Mn ions (*i.e.*, dimer). Thus, throughout this work, we shall consider the Q Mn ions paired as $Q/2$ dimers and estimate the effective AFM coupling constant by the mean value as

$$J_M \approx \frac{\frac{J_{MM}^{(0)} Q}{2}}{\frac{Q(Q-1)}{2}} = \frac{J_{MM}^{(0)}}{Q-1} \text{meV}$$

where $J_{MM}^{(0)} = 0.5$ meV is the coupling constant between nearest neighbor Mn ions in CdSe.[7,8,25] The model of eq 1 is extendible for more delicate consideration of various types of Mn aggregations (dimers, trimers, *etc.*) by including more corresponding spin−spin coupling terms and solved in a similar manner. However, for the purpose to confirm and physically analyze the existing AFM behind the experimental observations, the model of eq 1 should be sufficiently useful.

Since the Hamiltonian of eq 1 commutes with the operators of total spin of all Mn ions $\vec{\text{m}}_N \equiv \sum_{i=1}^{N} \vec{\text{m}}_i$, M_N^2 and M_N^z, and those of total spin of all AFM-interacting Mn ions ($\vec{\text{m}}_Q \equiv \sum_{i=1}^{Q} \vec{\text{m}}_i$), M_Q^2, the eigen-states can be represented by $|M_N, M_Q, M_N^z\rangle$. Correspondingly, eigen-energies are solved as

$$E(M_N, M_Q, M_N^z) = \frac{J_M}{2}\left(M_Q(M_Q+1) - \frac{35}{4}Q\right) - M_N^z g_{\text{Mn}} \mu_B B \quad (2)$$

According to eq 2, the magnetization and magnetic susceptibility of a Mn-doped NC supposedly can be calculated, which are $\mathbf{M} = -(\partial F/\partial B)_T = kT(\partial \ln Z/\partial B)$

and $\chi = (\partial \mathbf{M}/\partial B)$, defined in terms of the partition function

$$Z = \sum_{M_N, M_Q, M_N^z} n_{(M_N, M_Q, M_N^z)} e^{-E(M_N, M_Q, M_N^z)/kT} \quad (3)$$

as a function of the level energies $E(M_N, M_Q, M_N^z)$ and the degeneracies $n_{(M_N,M_Q,M_N^z)}$, as well. In practice, the degeneracies $n_{(M_N,M_Q,M_N^z)}$ are usually tremendously high (which are typically $n \gg 10^2$ for few Mn ions and even as many as $n > 10^{36}$ for ~75 Mn ions, as shown in Figure S1 of SI) to count out either analytically or numerically. One should note that, even though the model Hamiltonian of eq 1 is solvable, the magnetism of a Mn-doped NC cannot be calculated if the degeneracies of the energy spectrum remain unknown. The theoretical model and techniques presented here are, in general, applicable for any magnetic nanostructures containing a finite number of magnetic ions, including other colloidal nanostructures and self-assembled quantum dots under extensive studies.[26−29]

A key theoretical progress made here is the exploitation of group theory technique to make the $n_{(M_N,M_Q,M_N^z)}$ degeneracies of NCs countable with an arbitrary number of magnetic ion dopants, with no need for heavy numerical computation. Details of the group theory technique used for counting the high spin degeneracies are presented in the SI. By using the method, the complete energy spectra, including the level energies and degeneracies, of the measured magnetic NCs (including the ones doped with maximally 75 Mn ions per NC) in this work are calculated.

Analysis of *B*-Dependent Magnetism. In theoretical analysis, we begin with the *B*-dependent magnetism of CdSe:Mn NCs doped with distant paramagnetic Mn ions only (*i.e.*, $P \neq 0$, $Q = 0$), among which the Mn−Mn interactions are nearly vanishing. Figure 2a−c shows the calculated energy spectrum, magnetization, and magnetic susceptibility as functions of the magnetic field *B* for the magnetic NC of diameter $d = 5$ nm, doped with four distant Mn ions ($P = 4$, $Q = 0$, and $N = 4$). In Figure 2a, the ground states of the four Mn-doped NCs are shown to be those of the fixed (maximum) angular momentum $M_N = 10$ against the varied magnetic field. In these cases, the effective Hamiltonian (eq 1) can be recovered to that of the ideal paramagnet with $\mathbf{M} = g_{Mn}(NJ)B_J(g_{Mn}\mu_B B/kT)$ with $J = 5/2$ and $N = 4$. In the low field limit ($g_{Mn}\mu_B B/kT \ll 1$), $\mathbf{M} \approx J(J+1)N(g_{Mn}\mu_B)^2 B/3kT$ and $\chi \approx J(J+1)N(g_{Mn}\mu_B)^2/3kT$ obeys Curie's law well.[30,31] Remarkably, the latter formalism shows that the product of magnetic susceptibility and temperature, $\chi T \propto J(J+1)N$, is invariant with varied temperature and reflects the magnitude of the total angular momentum *J*.

Next, let us introduce additional AFM-interacting aggregative Mn ions into the Mn-doped NCs (*i.e.*, $Q \neq 0$). Figure 2d shows the energy spectrum of the same NC as considered in Figure 2a but with four additional

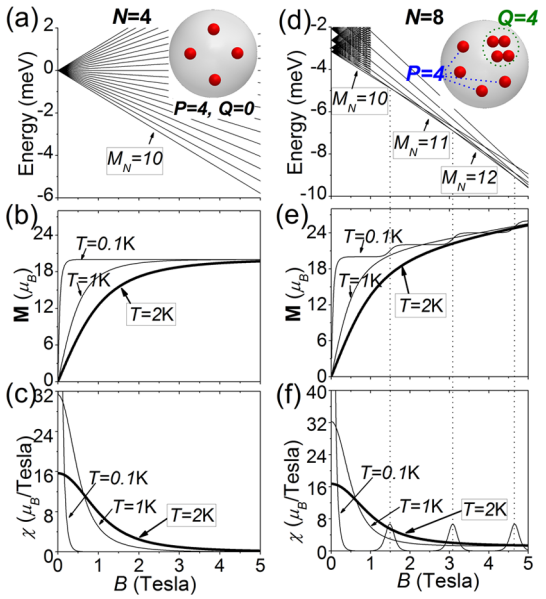

Figure 2. (a−c) Calculated energy spectrum, magnetization, and magnetic susceptibility of a magnetic CdSe:Mn NCs with four distant Mn ions ($P = 4$, $Q = 0$). (d−f) Calculated results for the same magnetic CdSe:Mn NCs but with four distant Mn ions ($P = 4$) and four additional aggregative Mn ions ($Q = 4$). Due to AFM interactions between the aggregative Mn ions, the ground states of the CdSe:Mn NCs possess the minimized total angular momentum ($M_N = 10$) at $B = 0$ and then undergo successive increments of angular momentum ($M_N = 10, 11, 12...$) with increasing applied magnetic field.

AFM-interacting Mn ions ($P = 4$, $Q = 4$, and $N = 8$). At zero or sufficiently small magnetic field, the total spin of the *Q* aggregative Mn ions that are subjected to AFM interactions vanishes and the total angular momentum of the ground states of the NC remains the same ($M_N = 10$) as that of the NC with $P = 4$ and $Q = 0$ shown in Figure 2a. Figure S1 shows the degeneracies (at the scales of 10^2-10^3) of the low-lying states (ordered by energy and also labeled with their quantum numbers M_N) of the eight Mn-doped NCs at zero magnetic field, which are calculated using the efficient group theory technique as presented in the SI and confirmed numerically. In contrast to the NC with $Q = 0$ (see Figure 2a), the ground states of the magnetic NC with $Q = 4$ AFM-interacting Mn ions (see Figure 2d) undergo successive increments of the angular momentum ($M_N = 10, 11, 12,...$) with increasing *B*, corresponding to the increments of the total spin of the aggregative Mn ions ($M_Q = 0, 1, 2,...$). As well-studied previously in refs 10, 12, and 32, the *B*-driven successive increments of the angular momentum of the AFM system result in the step feature of **M** and oscillating χ over a wide range of *B* at low *T*, as also seen in Figure 2e,f.

However, such an essential difference between the magnetic features of the NCs with and without AFM-interacting Mn ions at low *T* is likely smeared out by thermal fluctuations. As shown in Figure 2e,f, the step feature of **M** and the corresponding oscillating χ of the

NCs doped with aggregative Mn ions are completely faded out as the temperature is increased to $T = 2$ K and become indistinguishable from those of the NC without any aggregative Mn ions (see curves for $T = 2$ K in Figure 2b,c).

Figure 3a shows the measured magnetic susceptibility of the MCS804 NC sample at $T = 2$ K as a function of the magnetic field and, for comparison, the theoretical results of the magnetic NCs with fixed $P = 4$ distant Mn ions and varied number ($Q = 0, 2, 4$) of aggregative Mn ions. One sees that all of the NCs undoped or doped with a different number of aggregative Mn ions exhibit similar B dependences on magnetism at $T = 2$ K. Therefore, simply from the B-dependent magnetism, one cannot judge the existence and even infer the number of aggregative Mn ions in a magnetic-ion-doped NC.

Analysis of *T*-Dependent Magnetism. Alternatively, we suggest studying the AFM established between aggregative Mn ions in the magnetic NCs by analyzing the product of χT as a function of the temperature T. Another way often advised by standard AFM theory is by means of examining the T dependence of the magnetic susceptibility, χ *versus* T. Nevertheless, as presented in Figure S2 and discussed in the SI, the usefulness of the $\chi - T$ analysis is limited for the CdSe:Mn NCs studied here since only part of Mn ions in Mn-doped NCs are aggregated and AFM-interacting.

Figure 3b presents the measured χT values of the MCS804 sample at the varied temperatures from $T = 2$ to 200 K, which are not shown invariant with respect to the varied T as predicted by Curie's law. To understand the observed feature, we calculate the χT values as functions of T for the NCs with various mixtures of distant and aggregative Mn ions, ($P = 4$, $Q = 0$), ($P = 4$, $Q = 2$), ($P = 4$, $Q = 4$), and ($P = 8$, $Q = 0$). For the NCs without any aggregative Mn ions ($P = 4$, $Q = 0$ and $P = 8$, $Q = 0$), the values of the calculated χT remain unchanged with respect to the varied T and are determined by the number of P. Adding aggregative Mn ions to the NC (Q = 2,4), the calculated χT values become T-dependent, which increase with T and gradually approach the maximum values as $T > 100$ K.

As mentioned previously, the magnitude of χT of a magnetic system is associated with the total angular momentum of the system in Curie's law. At extremely low T, because of the existing AFM interactions, the angular momentum of the ground states of a magnetic NC with $Q \neq 0$ is minimized, where the spins of the individual aggregative Mn ions are antiparallel. This leads to the lowest value of χT at $T \rightarrow 0$, as shown in Figure 3b for the cases of ($P = 4$, $Q = 2$) and ($P = 4$, $Q = 4$). With increasing T, the NCs could thermally access more excited states of higher angular momentum, and the χT gradually increases. At very high T (such as $T >$ 100 K), all states of various angular momenta are nearly equally accessed and the χT eventually approaches a saturated value. One thus realizes that, unlike the B-dependent magnetism, the T dependences of χT of the NCs with different P and Q are quite distinct. This allows us to identify and distinguish AFM-interacting Mn aggregations from the overall paramagnetism of a CdSe:Mn NC sample by examining the T dependence of the measured χT.

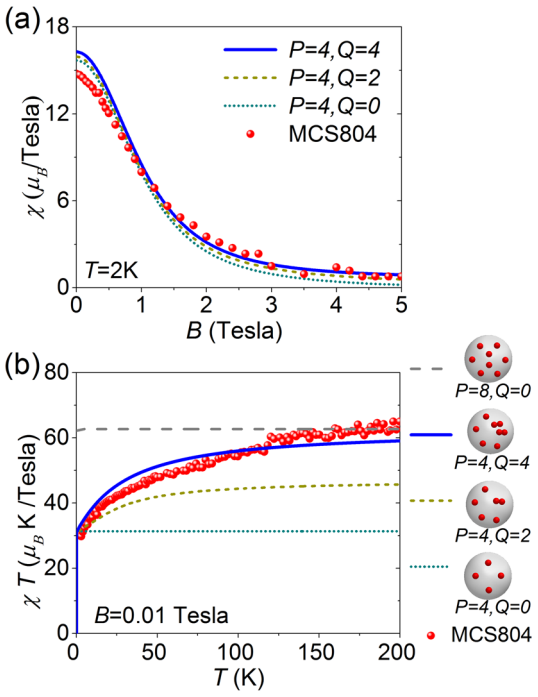

Figure 3. (a) Measured susceptibility χ of the sample MCS804 at $T = 2$ K as a function of magnetic field and the simulated results of the NCs with four fixed distant Mn ions ($P = 4$) but various numbers of aggregative Mn ions ($Q = 0, 2, 4$). The simulation shows that, even at the low temperature, the B-dependent magnetic susceptibility of a NC is insensitive to the variation of the number of AFM-interacting aggregative Mn ions and difficult to show the underlying AFM in the paramagnetic NCs with Mn aggregations. (b) Measured product of magnetic susceptibility and temperature, χT, of the sample MCS804 at $B = 0.01$ T *versus* the varied temperature. The simulated results of the NCs with $P = 4$ and $Q = 0$, 2, and 4 are presented to fit the experimental data. Note that the T dependence of the measured χT is very sensitive to the portions of the distant and aggregative Mn ions, and by fitting the T-dependent χT, one can infer the most possible (P,Q) of a magnetic-ion-doped NC. In this case, the simulated result for $P = 4$ and $Q = 4$ shows the best fitting.

In Figure 3b, the theoretical curve of ($P = 4$, $Q = 4$) is shown to best fit the experimental data of the MCS804 sample. Correspondingly, the estimated Mn concentration from the fitting of the T dependence of the measured χT is $x_T = N_T/N_{Cd} = 0.16\%$, which lies between $x_{dop} = N_{dop}/N_{Cd} = 0.375\%$ and $x_{eff} = N_{eff}/N_{Cd} = 0.09\%$, which are estimated from the supplied amount of dopant and fitting of B-dependent magnetism, respectively. Following the same fitting analysis, the sample MCS515 [MCS815] is inferred to contain ~8 [~75] Mn ions composed of $P = 5$ and $Q = 3$ [$P = 25$ and $Q = 50$], yielding the corresponding Mn concentration

x_T = 0.66% [x_T = 1.50%], as shown in Figure 4a,b [Figure 4c,d]. Remarkably, the high degeneracies, as many as ~10^{36} (see Figure S1b), of the energy spectrum of the NCs doped with 75 Mn ions need to be determined precisely in the calculation of magnetization and can be counted out only by using the efficient group theory technique. One also notes that the measured χT values of the NC ensembles persistently descend with increasing temperature, T > 100 K. The observed linearly descending feature of χT could be attributed to the inherent diamagnetism of host material CdSe,[33,34] which was not considered in the model. The temperature-insensitive diamagnetism makes a negative constant offset to the total magnetic susceptibility and leads to a linear descending χT (see section S4 in the SI for more details).

Figure 5 summarizes and compares the estimated numbers of Mn ions per NC by different means. Among the three estimated numbers of Mn ions for a sample, N_{dop} always shows the highest number since N_{dop} counts not only the Mn ions aggregated but also the ones not really incorporated into the NCs. By contrast, the values of N_{eff} are always the smallest because N_{eff} counts only the spatially distant Mn ions but might overlook all aggregative Mn ions that are often magnetically inactive. As best estimated numbers, N_T values lie usually between the numbers N_{dop} and N_{eff} for the same NC sample since N_T values rule out that the Mn ions are not really doped into the NCs but take into account both the spatially distant and aggregated Mn ions.

Charging Effects. Another advantageous feature of magnetic NCs is the charge-controlled magnetism. Charging a magnetic-ion-doped NC creates quantum-confinement enhanced spin interactions between confined charge carriers and Mn ions which tend to maximize the magnetism of the NC. Experimentally, Ochsenbein *et al.*[35,36] have presented the charge-controlled magnetism of $Zn_{1-x}Mn_xO$ NCs. By extending the employed model for uncharged Mn-doped NCs, the Hamiltonian of a singly charged NC doped with many Mn ions is given by

$$H_{eM}^{eff} = -J_c\vec{s}\cdot\sum_{i=1}^{N}\vec{m}_i + \frac{J_M}{2}\sum_{i(\neq j)=1}^{Q}\sum_{j=1}^{Q}\vec{m}_i\cdot\vec{m}_j - l_z g_L\mu_B B \quad (4)$$

where the first term represents the magnetic couplings between the quantum-confined electrons and all magnetic ions in the NC; the second one is the magnetic couplings between aggregative Mn ions, and the last one is the spin Zeeman term, $\vec{s}(s = 1/2)$, denoting the spin of charging electron, $\vec{l} = \vec{s} + \vec{M}_N(l_z)$ is the total spin (the z-component of the total spin) of electron and Mn ions, and g_L is the Lande g-factor.

The strength of the magnetic coupling is quantum-confinement engineerable and estimated by $J_c = 6J_{eM}^{(0)}/(\pi d^3)$ meV with $J_{eM}^{(0)}$ = 10.8 meV nm^3 in the spherical hard wall model for CdSe:Mn NCs.[5,37] Since the effective Hamiltonian of eq 4 commutes with the spin operators, I^2, I_z, M_N^2, and M_Q^2, the eigen-states can be represented by the corresponding quantum numbers, that is, $|I, M_N, M_Q, I_z\rangle$, and the energy spectrum is explicitly solved as

$$E(I, M_N, M_Q, I_z) = -\frac{J_c}{2}\left(\frac{1}{2}\pm\left(M_N - \frac{1}{2}\right)\right) + \frac{J_M}{2}\left(M_Q(M_Q+1) - \frac{35}{4}Q\right) - I_z g_L\mu_B B$$

where the up/down signs (±) correspond to $I = M_N + s$ and $I = M_N - s$, respectively. The magnetizations and magnetic susceptibilities of singly charged Mn-doped

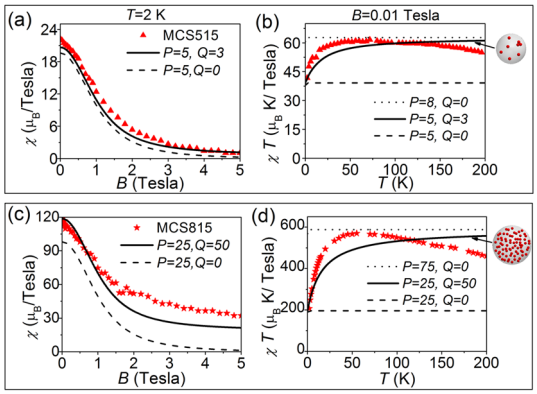

Figure 4. (a) Measured magnetic susceptibility χ, as a function of B, of the sample MCS515 at T = 2 K and (b) measured χT, as a function of T, of the same samples at B = 0.01 T. Correspondingly, the theoretical results for the NCs with various numbers of distant and aggregative Mn ions are presented in the plots to fit the experimental data. (c,d) Measured and theoretical results of the MCS815 sample, composed of the NCs doped with a high number of Mn ions, under the same conditions as (a) and (b). As a result of the fitting, the NCs in the MCS515 (MCS815) sample are inferred to contain, on average, 5 (25) distant Mn ions and 3 (50) aggregative Mn ions.

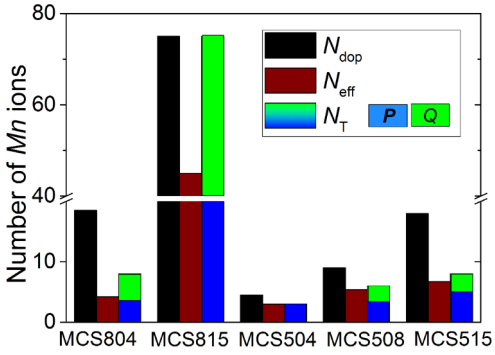

Figure 5. Statistics of the average numbers (N_{dop}, N_{eff}, and N_T) of Mn ions per NC of the CdSe:Mn NC samples MCS504, MCS508, MCS515, MCS804, and MCS815, which are estimated by three different means. The number of total Mn ions (N_T), composed of the aggregative Mn ions (Q) and distant Mn ions (P), for a NC is deduced from the best fittings of the T dependence of the χT, as presented in Figures 3b and 4b,d.

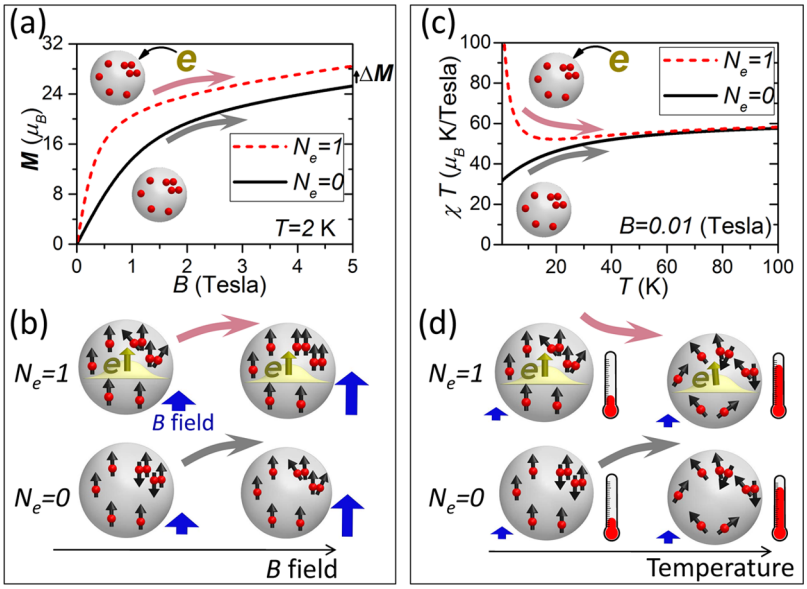

Figure 6. (a) Calculated magnetizations as functions of magnetic field *B* of a magnetic NC of diameter *d* = 5 nm doped with eight Mn ions composed of (*P* = 4, *Q* = 4) uncharged (black solid line) and charged with a single electron (red dashed line). The inset (b) illustrates how the spins of aggregated Mn ions and the resulting magnetization of a magnetic NC increase with increasing *B* whether the NC is charged or not. (c) Calculated product of temperature and magnetic susceptibilities, χT, of the uncharged (black solid line) and singly charged (red dashed line) magnetic NCs with fixed magnetic field *B* = 0.01 T but varied temperature *T*. The inset (d) illustrates that the spin alignments of Mn ions and the resulting magnetism of uncharged and charged magnetic NCs evolve in distinctive ways against the varied *T*.

NCs can be calculated following the same approach used previously for uncharged CdSe:Mn NCs.

Figure 6a shows the calculated magnetizations of charged and uncharged CdSe:Mn NCs with $P = 4$ and $Q = 4$ Mn ions as functions of the magnetic field. One sees that charging an electron onto a CdSe:Mn NC increases the magnetization overall, but a B dependence very similar to that of the uncharged one remains. This is because the electron−Mn couplings act as an additional effective field and polarize the spins of aggregative Mn ions. However, the electron−Mn couplings are weakly B-dependent and do not alter much the B-dependent feature of the magnetization. Figure 6b illustrates why the magnetization of charged NCs is overall larger than that of uncharged NCs. Thus, *via* single measurements on the B-dependent magnetism of a magnetic NC, one still cannot judge if the NC is charged or uncharged and further identify the charging effects on the magnetism.

Again, we suggest that analyzing the T dependence of the quantity χT is an excellent way to identify the charging effect on the enhanced magnetism of a magnetic-ion-doped NC. Figure 6c shows the calculated χT values of the uncharged and singly charged magnetic NCs with $P = 4$ and $Q = 4$ Mn ions. It is observed that the charged CdSe:Mn NC exhibits a T dependence of χT essentially different from that of the uncharged NC. While the calculated χT of an uncharged NC shows a monotonically increasing feature with increasing T, the same NC charged with a single electron shows a much greater value of χT at the lowest T and then, contrarily, a dramatic decrease with increasing T. The contrast between the T-dependent magnetic features of χT of a charged and an uncharged magnetic-ion-doped NC allows us to unambiguously identify the charge-enhanced magnetism of a magnetic ion NC. Figure 6d illustrates how charging a magnetic NC leads to the drastically different T dependence of χT. At low B and T (where $\mu_B B, kT < J_M \sim 0.5$ meV), the spins of the distant Mn ions are fully polarized by the external B field, while the total spin of the aggregative Mn ions is minimized due to the AFM interactions. In the charged NCs, the electron−Mn interactions that act as a huge effective field to Mn ions might make the spins of the aggregative Mn ions partially polarized, as schematically shown by the NC for low T and $N_e = 1$ in Figure 6d. As a result, the χT of the charged NC at low T is much higher than that of uncharged NC, as seen in Figure 6c. With increasing temperature, the thermal effect tends to depolarize the polarized spins of the distant Mn ions and the aggregative ones, as well, in the charged NC, and the resulting χT decreases. In contrast, the spins of the aggregative Mn ions in the uncharged NCs are unpolarized due to the AFM interactions. Increasing temperature tends to polarize the spins of the aggregative Mn ions in the uncharged NCs because the high spin states of the aggregative Mn ions lie at higher energy and are accessed thermally. Thus, even though the spins of distant Mn ions are subjected to the same thermal depolarization effect, the overall χT slightly increases with increasing T, showing a feature of

T dependence of χT totally different from that of the charged NC.

CONCLUSION

In summary, we present the experimental and theoretical investigation of the magnetism of CdSe:Mn nanocrystals. For physical analysis of the magnetic NCs doped with magnetic ion dopants whose spatial distribution and numbers are essentially random and statistical, we propose a solvable model Hamiltonian that can deal with the interacting Mn spins individually for an arbitrary number of Mn ions and establish an analysis method for revealing the underlying AFM established between aggregated Mn ions in paramagnetic Mn-doped NCs. By fitting the observed temperature-dependent magnetic susceptibilities, χT, with theoretical calculations, we clearly reveal the signatures of anti-ferromagnetism established between short-range interacting Mn aggregation of CdSe:Mn nanocrystals that are usually well hidden in the pronounced paramagnetism and hard to expose. It is shown that in our magnetic NC samples about 0−60% of magnetic ions aggregate and significantly reduce the total magnetizations. Moreover, we also show that analyzing the T dependence of χT is an excellent way to identify the charge-controlled magnetism of a magnetic-ion-doped nanocrystal, another remarkably advantageous feature of magnetic nanostructures in applications of spintronics and nanomagnetism.

METHODS

Sample Preparation. The uniformity of NC size was controlled by growth time and further improved by a size selection procedure.[24] The crystalline structures, the morphology of the spherical shapes, and the sizes of the NCs were confirmed from the high-resolution transmission electron microscope images, as shown in the abstract graphic. Accordingly, the NC size distributions are confirmed to have a variation within a small standard deviation of only 7% for all of the samples, and the high-quality crystalline structures of NCs are not affected by the doping of Mn ions. It is also confirmed that the sizes of the NCs and the Mn concentrations are uncorrelated. More detailed information about the sample synthesis and characterizations can be found in section S3 in the Supporting Information.

Measurements. Magnetizations of $Cd_{1-x}Mn_xSe$ NCs were measured by a superconducting quantum interference device over the temperature ranges from 2 to 200 K and magnetic fields from 0 to 5 T. The as-grown $Cd_{1-x}Mn_xSe$ NCs stabilized with capping agents of both trioctylphosphine and oleic acid, whose magnetizations are much smaller than those of bulk $Cd_{1-x}Mn_xSe$, are negligible. To extract the magnetization of CdSe:Mn NCs from the measured data, we subtracted only the sample holder background (mainly the capsule), which is about -1×10^{-6} emu at 0.1 T.

Conflict of Interest: The authors declare no competing financial interest.

Acknowledgment. This work was supported by the National Science Council of Taiwan under Contract No. NSC-100-2112-M-009-013-MY2 and the Center for Interdisciplinary Science (CIS) at National Chiao Tung University. The authors thank Jiye Fang (State University of New York at Binghamton) for providing the nanocrystal materials. S.J.C. is grateful to the National Center for Theoretical Science for support.

Supporting Information Available: Detailed description for the theoretical method based on group theory techniques of efficient counting of degeneracies of the energy spectrum a magnetic NC doped with arbitrary number of magnetic ions, calculation and analysis of temperature-dependent magnetic susceptibilities of magnetic NCs with AFM-interacting aggregative magnetic ions, and estimation of the diamagnetisms in the measured CdSe:Mn nanocrystals. This material is available free of charge *via* the Internet at http://pubs.acs.org.

REFERENCES AND NOTES

1. Wolf, S. A.; Awschalom, D. D.; Buhrman, R. A.; Daughton, J. M.; von Molnar, S.; Roukes, M. L.; Chtchelkanova, A. Y.; Treger, D. M. Spintronics: A Spin-Based Electronics Vision for the Future. *Science* **2001**, *294*, 1488–1495.
2. Hedin, E. R.; Joe, Y. S. *Spintronics in Nanoscale Devices*; Pan Stanford Publishing: Singapore, 2013.
3. Awschalom, D. D.; Bassett, L. C.; Dzurak, A. S.; Hu, E. L.; Petta, J. R. Quantum Spintronics: Engineering and Manipulating Atom-like Spins in Semiconductors. *Science* **2013**, *339*, 1174–1179.
4. Dietl, T.; Ohno, H. Dilute Ferromagnetic Semiconductors: Physics and Spintronic Structures. *Rev. Mod. Phys.* **2014**, *86*, 187–251.
5. Cheng, S. J. Theory of Magnetism in Diluted Magnetic Semiconductor Nanocrystals. *Phys. Rev. B* **2008**, *77*, 115310.
6. Cheng, S. J. Magnetic Anisotropy in Symmetric Magnetic Colloidal Quantum Dots Doped with Few Mn^{2+} Impurities. *Phys. Rev. B* **2009**, *79*, 245301.
7. Qu, F.; Hawrylak, P. Magnetic Exchange Interactions in Quantum Dots Containing Electrons and Magnetic Ions. *Phys. Rev. Lett.* **2005**, *95*, 217206.
8. Qu, F.; Hawrylak, P. Theory of Electron Mediated Mn-Mn Interactions in Quantum Dots. *Phys. Rev. Lett.* **2006**, *96*, 157201.
9. Abolfath, R. M.; Hawrylak, P.; Zutic, I. Tailoring Magnetism in Quantum Dots. *Phys. Rev. Lett.* **2007**, *98*, 207203.
10. Shapira, Y.; Bindilatti, V. Magnetization-Step Studies of Antiferromagnetic Clusters and Single Ions: Exchange, Anisotropy, and Statistics. *J. Appl. Phys.* **2002**, *92*, 4155.
11. Shapira, Y.; Foner, S.; Becla, P.; Domingues, D. N.; Naughton, M. J.; Brooks, J. S. Nearest-Neighbor Exchange Constant and Mn Distribution in $Zn_{1-x}Mn_xTe$ from High-Field Magnetization Step and Low-Field Susceptibility. *Phys. Rev. B* **1985**, *33*, 356–365.
12. Gratens, X.; Bindilatti, V.; Oliveira, N. F., Jr.; Shapira, Y.; Foner, S.; Golacki, Z.; Haas, T. E. Magnetization Steps in $Zn_{1-x}Mn_xO$: Four Largest Exchange Constants and Single-Ion Anisotropy. *Phys. Rev. B* **2004**, *69*, 125209.
13. Gaj, J. A.; Planel, R.; Fishman, G. Relation of Magneto-optical Properties of Free Excitons to Spin Alignment of Mn^{2+} Ions in $Cd_{1-x}Mn_xTe$. *Solid State Commun.* **1979**, *29*, 435–438.
14. Zajac, M.; Gosk, J.; Kaminska, M.; Twardowski, A.; Szyszko, T.; Podsiadlo, S. Paramagnetism and Antiferromagnetic d-d Coupling in GaMnN Magnetic Semiconductor. *Appl. Phys. Lett.* **2001**, *79*, 2432–2434.
15. Lipinska, A.; Simserides, C.; Trohidou, K. N.; Goryca, M.; Kossacki, P.; Majhofer, A.; Dietl, T. Ferromagnetic Properties of p-(Cd,Mn)Te Quantum Wells: Interpretation of Magneto-optical Measurements by Monte Carlo Simulations. *Phys. Rev. B* **2009**, *79*, 235322.
16. Spalek, J.; Lewicki, A.; Tarnawski, Z.; Furdyna, J. K.; Galazka, R. R.; Obuszko, Z. Magnetic Susceptibility of Semimagnetic Semiconductors: The High-Temperature Regime and the Role of Superexchange. *Phys. Rev. B* **1986**, *33*, 3407.

17. Bergqvist, L.; Eriksson, O.; Kudrnovsk, J.; Drchal, V.; Korzhavyi, P.; Turek, I. Magnetic Percolation in Diluted Magnetic Semiconductors. *Phys. Rev. Lett.* **2004**, *93*, 137202.
18. Kudrnovsky, J.; Turek, I.; Drchal, V.; Maca, F.; Weinberger, P.; Bruno, P. Exchange Interactions in III−V and Group-IV Diluted Magnetic Semiconductors. *Phys. Rev. B* **2004**, *69*, 115208.
19. Xu, J. L.; Schilfgaarde, M.; Samolyuk, G. D. Role of Disorder in Mn:GaAs, Cr:GaAs, and Cr:GaN. *Phys. Rev. Lett.* **2005**, *94*, 097201.
20. Fernández-Rossier, J.; Brey, L. Ferromagnetism Mediated by Few Electrons in a Semi-magnetic Quantum Dot. *Phys. Rev. Lett.* **2004**, *93*, 117201.
21. Climente, J. I.; Korkusiski, M.; Hawrylak, P.; Planelles, J. Voltage Control of the Magnetic Properties of Charged Semiconductor Quantum Dots Containing Magnetic Ions. *Phys. Rev. B* **2005**, *71*, 125321.
22. Bhattacharjee, A. K.; Perez-Conde, J. Optical Properties of Paramagnetic Ion-Doped Semiconductor Nanocrystals. *Phys. Rev. B* **2003**, *68*, 045303.
23. Nguyen, N. T. T.; Peeters, F. Magnetic Field Dependence of the Many-Electron States in a Magnetic Quantum Dot: The Ferromagnetic−Antiferromagnetic Transition. *Phys. Rev. B* **2008**, *78*, 045321.
24. Jian, W. B.; Fang, J.; Ji, T.; He, J. Quantum-Size-Effect-Enhanced Dynamic Magnetic Interactions among Doped Spins in $Cd_{1-x}Mn_xSe$ Nanocrystals. *Appl. Phys. Lett.* **2003**, *83*, 3377–3379.
25. Furdyna, J. K. Diluted Magnetic Semiconductors. *J. Appl. Phys.* **1988**, *64*, R29–R64.
26. Long, G.; Barman, B.; Delikanli, S.; Tsai, Y. T.; Zhang, P.; Petrou, A.; Zeng, H. Carrier−Dopant Exchange Interactions in Mn-Doped PbS Colloidal Quantum Dots. *Appl. Phys. Lett.* **2012**, *101*, 062410.
27. Reshina, I. I.; Ivanov, S. V.; Toropov, A. A. Magneto-optical Studies of Ensembles of Semimagnetic Self-Organized Cd(Mn)Se/Zn(Mn)Se Quantum Dots. *Phys. Rev. B* **2012**, *86*, 155302.
28. Klopotowski, L.; Cywinski, L.; Szymura, M.; Voliotis, V.; Grousson, R.; Wojnar, P.; Fronc, K.; Kazimierczuk, T.; Golnik, A.; Karczewski, G.; Wojtowicz, T. Influence of Exciton Spin Relaxation on the Photoluminescence Spectra of Semimagnetic Quantum Dots. *Phys. Rev. B* **2013**, *87*, 245316.
29. Turyanska, L.; Hill, R. J. A.; Makarovsky, O.; Moro, F.; Knott, A. N.; Larkin, O. J.; Patane, A.; Meaney, A.; Christianen, P. C. M.; Fay, M. W.; Curry, R. J. Tuneable Paramagnetic Susceptibility and Exciton g-Factor in Mn-Doped PbS Colloidal Nanocrystals. *Nanoscale* **2014**, *6*, 8919–8925.
30. Blundell, S. *Magnetism in Condensed Matter*; Oxford University Press: New York, 2001.
31. Mattis, D. C. *The Theory of Magnetism Made Simple*; World Scientific Publishing: Singapore, 2006.
32. Bednarski, H.; Cisowski, J.; Portal, J. C. Magnetic Ion Statistics and Thermodynamics in Dilute Magnetic Semiconductor Quantum Structures. *Phys. Rev. B* **1997**, *55*, 15762–15767.
33. Neeleshwar, S.; Chen, C. L.; Tsai, C. B.; Chen, Y. Y.; Chen, C. C.; Shyu, S. G.; Seehra, M. S. Size-Dependent Properties of CdSe Quantum Dots. *Phys. Rev. B* **2005**, *71*, 201307.
34. Seehra, M. S.; Dutta, P.; Neeleshwar, S.; Chen, Y. Y.; Chen, C. L.; Chou, S. W.; Chen, C. C.; Dong, C. L.; Chang, C. L. Size-Controlled Ex-nihilo Ferromagnetism in Capped CdSe Quantum Dots. *Adv. Mater.* **2008**, *20*, 1656.
35. Ochsenbein, S. T.; Feng, Y.; Whitaker, K. M.; Badaeva, E.; Liu, W. K.; Li, X.; Gamelin, D. R. Charge-Controlled Magnetism in Colloidal Doped Semiconductor Nanocrystals. *Nat. Nanotechnol.* **2009**, *4*, 681–687.
36. Bussian, D. A.; Crooker, S. A.; Yin, M.; Brynda, M.; Efros, A. L.; Klimov, V. I. Tunable Magnetic Exchange Interactions in Manganese-Doped Inverted Core−Shell ZnSe−CdSe Nanocrystals. *Nat. Mater.* **2009**, *8*, 35–40.
37. Kacman, P. Spin Interactions in Diluted Magnetic Semiconductors and Magnetic Semiconductor Structures. *Semicond. Sci. Technol.* **2001**, *16*, R25–R39.